

## Oxidation Behavior of In-situ Synthesized MoSi<sub>2</sub>-SiC Composite at 700°C (Postprint)

**Authors:** Zhang Laiqi, Duan Lihui, Lin Junpin

**Date:** 2023-03-18T00:00:00+00:00

### Abstract

The long-term oxidation behavior of in-situ synthesized MoSi<sub>2</sub>-SiC composites with different SiC volume fractions was investigated at 700°C in air for 1000 h. The results show that after 1000 h of oxidation, none of the composites exhibited the pest phenomenon. The oxidation resistance of the composites was significantly better than that of monolithic MoSi<sub>2</sub>, and the oxidation resistance of the in-situ synthesized composites was superior to that of composites prepared by conventional hot-pressing of commercial MoSi<sub>2</sub> and SiC powder mixtures (ex-situ composites). The phase composition of the composite oxide scale was solely amorphous SiO<sub>2</sub>; the oxidation process of the material was primarily the reaction between O<sub>2</sub> and MoSi<sub>2</sub>, while SiC did not undergo oxidation. Simultaneous oxidation of silicon and molybdenum still occurred in the material at 700°C; due to the rapid volatilization of MoO<sub>3</sub>, no whisker formation occurred, thus a thin, continuous, and dense amorphous SiO<sub>2</sub> protective layer rapidly formed on the material surface, endowing the material with excellent long-term oxidation resistance.

### Full Text

#### Preamble

Vol. 29 No. 8

CHINESE JOURNAL OF MATERIALS RESEARCH

August 2015

#### Oxidation Behavior of In-situ Synthesized MoSi<sub>2</sub>-SiC Composites at 700°C

ZHANG Laiqi, DUAN Lihui, LIN Junpin

(State Key Laboratory for Advanced Metals and Materials, University of Science and Technology Beijing, Beijing 100083, China)

*Supported by National Natural Science Foundation of China No. 50871012 and National Basic Research Program of China No. 2011CB605502.*

### **Abstract**

The long-term air oxidation behavior of in-situ synthesized MoSi<sub>2</sub>-SiC composites with different volume fractions of SiC was investigated at 700°C for 1000 h. The results demonstrate that none of the composites exhibited pest disintegration after 1000 h of oxidation. The oxidation resistance of the composites was significantly superior to that of monolithic MoSi<sub>2</sub>, and the in-situ synthesized composites outperformed conventional composites prepared by hot-pressing mixtures of commercial MoSi<sub>2</sub> and SiC powders (ex-situ composites). The oxide scale formed on the composites consisted solely of amorphous SiO<sub>2</sub>, indicating that oxidation primarily involved the reaction between O<sub>2</sub> and MoSi<sub>2</sub>, while SiC remained unoxidized. At 700°C, simultaneous oxidation of silicon and molybdenum still occurred, but the rapid volatilization of MoO<sub>3</sub> prevented whisker formation, thereby enabling rapid formation of a thin, continuous, and dense amorphous SiO<sub>2</sub> protective layer on the material surface that conferred excellent long-term oxidation resistance.

### **Keywords**

materials failure and protection, MoSi<sub>2</sub>-SiC composite, in-situ synthesis, low-temperature oxidation behavior, pest phenomenon

---

## **Introduction**

MoSi<sub>2</sub> is a promising high-temperature structural material following nickel-based superalloys and TiAl intermetallic alloys, offering a high melting point (2030°C), low density (6.24 g/cm<sup>3</sup>), excellent high-temperature oxidation resistance, thermal conductivity comparable to metals, and a low coefficient of thermal expansion. However, its practical application has been limited by inadequate low-temperature toughness, insufficient high-temperature strength, and particularly the pest phenomenon (catastrophic oxidation where bulk material disintegrates into powder) that occurs at low temperatures. Fitzer first observed that monolithic MoSi<sub>2</sub> transforms from bulk to powder during oxidation in the 400–800°C range, causing catastrophic material failure. Consequently, research on the low-temperature oxidation performance of MoSi<sub>2</sub> and its composites has attracted considerable attention. Nevertheless, the mechanism underlying low-temperature pest oxidation remains controversial, with several competing theories: formation of volatile molybdenum oxides leading to discontinuous and porous SiO<sub>2</sub> protective films; initiation of pest phenomenon by pores and cracks in the material; preferential diffusion of gaseous elements (O or N) along grain boundaries; and dependence of pest phenomenon on material density and oxygen partial pressure. Based on these divergent views, numerous researchers have attempted to improve the low-temperature oxidation behavior of MoSi<sub>2</sub> through various approaches, including enhancing purity and density, modifying

microstructure, adding elements with oxygen affinity, incorporating reinforcing phases for composite strengthening, and high-temperature pre-oxidation to form dense  $\text{SiO}_2$  films. Despite these efforts, the oxidation mechanism of low-temperature pest phenomenon in  $\text{MoSi}_2$  remains unclear, and effective methods to mitigate or eliminate pest phenomenon are still lacking.

SiC has emerged as a primary reinforcement for  $\text{MoSi}_2$  due to its excellent thermodynamic and chemical compatibility with  $\text{MoSi}_2$  and its outstanding oxidation resistance. Composites prepared via in-situ synthesis benefit from clean, oxide-free interfaces with strong bonding, as the reinforcement forms within the matrix during processing. This uniform particle distribution enhances mechanical properties, particularly at elevated temperatures, making in-situ synthesis widely applicable for composite fabrication. Our research group has previously prepared  $\text{MoSi}_2$ -SiC composites using in-situ synthesis and conducted systematic investigations of their microstructure and mechanical properties, demonstrating significant improvements in low-temperature toughness, high-temperature strength, and creep resistance. However, oxidation behavior studies have only examined resistance at  $500^\circ\text{C}$ . Most existing research on  $\text{MoSi}_2$ -SiC composite oxidation has focused on high-temperature regimes, with limited investigation of low-temperature oxidation behavior and even fewer studies on long-term oxidation of in-situ synthesized composites. Since  $\text{MoSi}_2$  undergoes accelerated low-temperature oxidation leading to pest phenomenon in the  $400$ - $800^\circ\text{C}$  range, and our previously developed in-situ  $\text{MoSi}_2$ -SiC composites showed no pest phenomenon after 1000 h at  $500^\circ\text{C}$ , it remains necessary to examine whether pest occurs at other temperatures within this critical range. This study investigates the oxidation behavior of in-situ synthesized  $\text{MoSi}_2$ -SiC composites with varying SiC contents during 1000 h exposure to air at  $700^\circ\text{C}$  and explores the underlying oxidation mechanisms.

## Experimental

The experimental materials were in-situ synthesized  $\text{MoSi}_2$ -SiC composites with SiC volume fractions of 10%, 20%, 30%, and 45%, designated as MoSiC10, MoSiC20, MoSiC30, and MoSiC45, respectively. For comparison, monolithic  $\text{MoSi}_2$  (denoted MS) and a conventional  $\text{MoSi}_2$ -30%SiC composite prepared by hot-pressing a mixture of commercial  $\text{MoSi}_2$  and SiC powders (ex-situ composite, denoted WS) were also tested. Oxidation specimens measuring  $15\text{ mm} \times 10\text{ mm} \times 1\text{ mm}$  were cut from each material using Mo wire electrical discharge machining. The surfaces were ground to 1000-grit finish with metallographic sandpaper, ultrasonically cleaned in acetone, and dried.

Oxidation tests were conducted in a box furnace at  $700^\circ\text{C}$  in naturally convected air. To ensure full exposure of all six specimen surfaces to air, samples were placed obliquely in ceramic crucibles that had been pre-fired at  $950^\circ\text{C}$  for at least 48 h until mass variation was less than 0.0001 g. At regular intervals, samples were removed and cooled naturally, then weighed together with their crucibles using an electronic analytical balance (sensitivity:  $10^{-4}$  g). The total

oxidation duration was 1000 h.

Phase composition of the oxidized surfaces was analyzed using a Rigaku D-MAX X-ray diffractometer (XRD, Cu-K $\alpha$ ). Surface morphology and composition of the oxide scales were examined using a SUPRA 55 scanning electron microscope (SEM) with energy-dispersive spectroscopy (EDS). Surface phase composition was further characterized using a PHI Quantera X-ray photoelectron spectrometer (XPS) with a detection depth of only 2 nm, Al K $\alpha$  radiation (1486.6 eV), and a detection area of 300  $\mu\text{m} \times 300 \mu\text{m}$ . Full scans and narrow scans for each element were performed, with chemical states determined based on binding energy shifts. Charging effects were corrected using the C 1s binding energy of 284.6 eV. Overlapping peaks were deconvoluted using XPS peak software.

## Results

### 2.1 Oxidation Kinetics

Figure 1 [Figure 1: see original paper] presents the oxidation kinetic curves for the six materials after 1000 h at 700°C. All specimens exhibited minimal mass changes, which corresponded only to the incubation stage observed in the kinetic curves at 500°C, indicating strong oxidation resistance for all six materials at 700°C. During the initial 5 h (Figure 1c), all samples showed slight mass loss, attributed to evaporation of moisture and impurities from sample cleaning as well as volatilization of oxidation products. After 20 h, the mass of each sample began to increase to varying degrees (Figure 1b). The fluctuating trend in Figure 1c reveals that mass gain was not monotonic between 0–20 h, indicating concurrent oxide volatilization during oxidation. Beyond 20 h, the curves became relatively stable (Figure 1b). Subsequent curve fluctuations resulted from weighing errors (differences of only 0.1 mg/cm<sup>2</sup>). The six curves intersected without significant divergence, suggesting similar oxidation resistance among the materials. At 200 h, the maximum mass gain was only 0.31 mg/cm<sup>2</sup>, corresponding to an oxidation rate of 0.0016 mg/(cm<sup>2</sup> · h). At 500 h, the maximum mass gain was 0.4 mg/cm<sup>2</sup>, but the oxidation rate decreased to 0.0008 mg/(cm<sup>2</sup> · h), demonstrating progressively slower oxidation.

As shown in Figure 1a, the curves began to diverge after approximately 500 h, with monolithic MoSi<sub>2</sub> (MS) showing greater mass gain than the MoSi<sub>2</sub>-SiC composites, confirming superior oxidation resistance of the composites. The ex-situ WS composite exhibited larger mass changes compared to the in-situ MoSiC30, indicating that in-situ synthesized MoSi<sub>2</sub>-SiC composites possess higher oxidation resistance than ex-situ composites. After 1000 h, monolithic MoSi<sub>2</sub> showed the maximum mass gain of 0.37 mg/cm<sup>2</sup>, but the oxidation rate further decreased to 0.00037 mg/(cm<sup>2</sup> · h), nearly approaching zero compared to the 0.15 mg/(cm<sup>2</sup> · h) rate observed at 500°C. These results demonstrate that significant mass changes and severe oxidation occurred only during the first 20 h, accompanied by oxide volatilization, while subsequent oxidation remained relatively stable with minimal volatilization. Overall, the kinetic curves for all six mate-

rials showed minimal variation at 700°C, and all materials exhibited excellent long-term oxidation resistance after 1000 h.

## 2.2 Oxide Film Phase Composition

Figure 2 [Figure 2: see original paper] shows the XRD patterns of MoSiC30, MS, and WS after 1000 h oxidation. The diffraction peaks corresponded primarily to MoSi<sub>2</sub> and SiC from the substrate matrix, with no oxide peaks or amorphous halos detected, confirming that the oxide film was too thin for XRD detection (typical XRD penetration depth ~10 nm).

Since XPS can detect phase composition within the top few nanometers of the oxide film, samples MS, MoSiC10, and MoSiC30 oxidized for 1000 h were analyzed by XPS, with results shown in Figure 3 [Figure 3: see original paper]. The Si 2p narrow-scan spectra revealed nearly identical binding energies of 103.3 eV for all three samples, corresponding to amorphous SiO<sub>2</sub>. The Mo 3d narrow-scan spectra showed low peak intensities, with atomic fractions of Mo (Table 1) that were essentially negligible (detection limit ~0.5%). The absence of distinct peaks indicated that molybdenum oxides were virtually absent on the oxide film surface. Combined with the kinetic data, this suggests that oxidation products were volatile and completely evaporated during oxidation. However, sample MS exhibited a relatively higher Mo atomic fraction with a binding energy peak at 232.8 eV, corresponding to MoO<sub>3</sub>, indicating trace amounts of unvolatilized MoO<sub>3</sub> remained on the MS surface. Nevertheless, based on the spectral characteristics, the Mo 3d binding energy peaks were negligible, and the atomic fraction values were at the detection limit, allowing complete disregard for MoO<sub>3</sub> formation on the oxide film surface.

Further analysis of the O 1s narrow-scan spectra showed nearly identical binding energy peaks for all three samples at 532.2 eV, corresponding to amorphous SiO<sub>2</sub>, consistent with the Si 2p analysis. These XPS results demonstrate that after 1000 h oxidation at 700°C, Si and Mo in the substrate surface were simultaneously oxidized to Si<sup>4+</sup> and Mo<sup>6+</sup>. The oxidation product MoO<sub>3</sub> completely volatilized over time, leaving the oxide film surface entirely covered by an amorphous SiO<sub>2</sub> layer (Table 1). This continuous, dense SiO<sub>2</sub> protective film hindered further oxygen diffusion and provided excellent protection to the substrate, resulting in negligible weight changes even after 1000 h oxidation and demonstrating outstanding long-term oxidation resistance.

## 2.3 Macroscopic Morphology of Oxide Film

Figure 4 [Figure 4: see original paper] presents the macroscopic surface morphologies of the six samples after 1000 h oxidation at 700°C. The appearance differed markedly from that observed at 500°C. A thin black oxide film formed on all sample surfaces, completely obscuring the substrate color. Visually, the oxide film appeared dense, crack-free, and without spallation, indicating significantly better oxidation resistance at 700°C compared to 500°C.

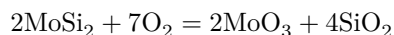
## 2.4 SEM Surface Morphology of Oxide Film

Figure 5 [Figure 5: see original paper] shows SEM images of the oxide film surfaces on the six samples after 1000 h oxidation at 700°C. Consistent with XPS results, all surfaces were covered by a thin amorphous SiO<sub>2</sub> layer. The dense oxide film showed no cracks (Figure 5), providing effective protection by blocking oxygen diffusion inward and yielding excellent oxidation performance. Although XPS indicated identical phase compositions, closer SEM examination revealed subtle morphological differences. The oxide surfaces of MoSiC30, MoSiC45, and WS clearly retained the original substrate microstructure, with black SiC particles uniformly distributed in the gray MoSi<sub>2</sub> matrix. Particularly, the SiC particles remained intact and clearly defined, showing no changes. This is because SiC oxidation begins around 800°C, and at the lower temperature of 700°C, SiC exhibited strong inertness toward oxygen, corroborating the SEM observations and indicating an extremely thin oxide film. In contrast, the surfaces of MoSiC10, MoSiC20, and MS showed nearly complete loss of the original substrate microstructure. MoSiC10 and MoSiC20 developed extensive black regions, and the gray MoSi<sub>2</sub> areas became rough and uneven, though SiC particles remained intact (Figure 5a). The monolithic MS surface consisted almost entirely of rough, uneven gray MoSi<sub>2</sub> regions. These morphological differences indirectly reflect variations in oxidation resistance, with MoSiC30, MoSiC45, and WS showing better performance than MS, MoSiC10, and MoSiC20, consistent with the kinetic curves. Overall, the oxide films on all six materials were very thin, with grinding scratches from sample preparation still visible (Figure 5a, f), demonstrating excellent oxidation resistance. Additionally, spherical particles observed on the oxide surfaces in Figures 5b, d, and f likely resulted from volatilization of the oxidation product MoO<sub>3</sub> during film formation.

## Discussion

### 3.1 Oxidation Mechanism Analysis

Chou et al. [2, 22] and Meschter [23] reported that simultaneous oxidation of Mo and Si in MoSi<sub>2</sub> at low temperatures follows the reaction:



Thermodynamic analysis confirms this reaction can proceed at 700°C, with the same reaction formula as at 500°C. The experimental results demonstrate that all six materials exhibited excellent oxidation resistance after 1000 h at 700°C, contrasting sharply with behavior at 500°C. To explain this significant difference for the same material at different temperatures, the oxidation mechanism at 700°C must be analyzed. During the initial oxidation stage at 700°C, the large contact area between the material surface and oxygen resulted in high oxygen partial pressure, and without selective oxidation of Mo or Si, MoSi<sub>2</sub> reacted directly with O<sub>2</sub> according to reaction (1) to form MoO<sub>3</sub> and amorphous SiO<sub>2</sub>.

The SiC in the matrix did not participate in the reaction, as SiC oxidation begins around 800°C [21], and at the lower temperature of 700°C, SiC remained inert toward oxygen, consistent with the SEM observations in Figure 5. This indicates that the oxidation process primarily involved the reaction between oxygen and MoSi<sub>2</sub>.

Parthasarathy et al. [24] demonstrated that MoO<sub>3</sub> forms during oxidation at temperatures as low as 350°C and begins to volatilize around 500°C, melting at 800°C. Therefore, at 700°C, MoO<sub>3</sub> formation was accompanied by continuous volatilization, similar to oxidation at 500°C. However, unlike oxidation at 500°C, the faster volatilization rate of MoO<sub>3</sub> at 700°C prevented whisker formation throughout the oxidation process. This is because MoO<sub>3</sub> whisker formation requires accumulation to a critical concentration; whiskers only form when the vapor pressure of volatilizing MoO<sub>3</sub> at the oxide surface reaches the supersaturation required for whisker nucleation, which would disrupt the scale's integrity and prevent formation of a continuous protective film, resulting in poor oxidation resistance at 500°C [20]. At 700°C, the rapid volatilization of MoO<sub>3</sub> prevented whisker formation, allowing SiO<sub>2</sub> to cover an increasingly large surface area. This progressively hindered oxygen diffusion to the reaction interface, as reflected in the kinetic curves in Figures 1b and 1c. Figure 1c shows significant fluctuations in the kinetic curves between 0–20 h due to MoO<sub>3</sub> formation and volatilization, while Figure 1b indicates relatively stable oxidation after 20 h with continuous mass gain. This demonstrates rapid formation of the SiO<sub>2</sub> protective film, which covered most of the surface within approximately 20 h, increasingly impeding oxygen diffusion to the reaction interface. Although higher temperatures increased silicon migration rates to the reaction interface, oxygen diffusion remained dominant, maintaining high oxygen partial pressure at the reaction interface and resulting in simultaneous oxidation of silicon and molybdenum.

XPS analysis (Figure 3) confirmed that a continuous, dense SiO<sub>2</sub> protective film ultimately formed on the oxide surface, preventing further oxygen diffusion and providing excellent substrate protection. Consequently, even after 1000 h oxidation, material weight changes were negligible, demonstrating outstanding long-term oxidation resistance. Based on this analysis, a schematic diagram of the oxidation mechanism for MoSi<sub>2</sub>-SiC composites at 700°C is presented in Figure 6 [Figure 6: see original paper].

### 3.2 Effect of SiC Content on Oxidation Behavior

Comparison of the six materials revealed differences in oxidation resistance after approximately 500 h at 700°C. As shown in Figure 1, MS exhibited significantly greater mass gain than the MoSi<sub>2</sub>-SiC composites, indicating that SiC addition improved the oxidation resistance of MoSi<sub>2</sub>. The analysis above demonstrates that oxidation primarily involved the reaction between oxygen and MoSi<sub>2</sub>. SiC addition reduced the relative MoSi<sub>2</sub> content and decreased composite porosity compared to monolithic MoSi<sub>2</sub> [17, 18], thereby slowing oxidation and enhancing

oxidation resistance. XPS results showed trace amounts of unvolatilized  $\text{MoO}_3$  remained on the MS surface after 1000 h oxidation. These residual  $\text{MoO}_3$  phases disrupted formation of the continuous, dense  $\text{SiO}_2$  protective film, contributing to reduced oxidation resistance. The oxidation kinetic curves indicated minimal differences in oxidation resistance among the in-situ synthesized  $\text{MoSi}_2$ -SiC composites with varying SiC contents.

### 3.3 Effect of Processing on Oxidation Behavior

The experimental results revealed that after approximately 500 h, the mass gain of WS was significantly greater than that of  $\text{MoSiC30}$ , indicating superior oxidation resistance of the in-situ synthesized composite. This difference arises because the ex-situ WS composite exhibited larger SiC particle spacing, non-uniform spatial distribution, and significantly higher porosity compared to the in-situ  $\text{MoSiC30}$  [18, 19]. These factors provided diffusion pathways for oxygen, resulting in greater oxidation mass gain and lower oxidation resistance. Thus, in-situ synthesis of  $\text{MoSi}_2$ -SiC increased density, reduced porosity, and restricted oxygen diffusion, thereby improving low-temperature oxidation resistance.

## Conclusions

1. After 1000 h oxidation at  $700^\circ\text{C}$ ,  $\text{MoSi}_2$ -SiC composites demonstrated superior oxidation resistance compared to monolithic  $\text{MoSi}_2$ , and in-situ synthesized composites outperformed ex-situ composites. None of the materials exhibited pest phenomenon after 1000 h oxidation.
2. The oxide film on the composites consisted primarily of amorphous  $\text{SiO}_2$ , with trace unvolatilized  $\text{MoO}_3$  detected only on sample MS. The oxidation process primarily involved the reaction between oxygen and  $\text{MoSi}_2$ , while SiC remained unoxidized.
3. Simultaneous oxidation of silicon and molybdenum occurred at  $700^\circ\text{C}$ . However, rapid volatilization of  $\text{MoO}_3$  prevented whisker formation, enabling rapid development of a continuous, dense amorphous  $\text{SiO}_2$  protective film on the material surface that conferred excellent long-term oxidation resistance at  $700^\circ\text{C}$ .

## References

1. E. Fitzner, Molybdenum disilicide as high-temperature material, in: Proceedings of 2nd Plansee Seminar, edited by F. Benesovsky (Vienna, Springer, 1955) p.56
2. T. C. Chou, T. G. Nieh, New observations of  $\text{MoSi}_2$  pest at  $500^\circ\text{C}$ , Scripta Metallurgica et Materialia, 26(10), 1637(1992)
3. C. G. McKamey, P. F. Tortorelli, J. H. DeVan, C. A. Carmichael, A study of pest oxidation in polycrystalline  $\text{MoSi}_2$ , Journal of Materials Research,

- 7(10), 2747(1992)
4. J. H. Westbrook, D. L. Wood, "PEST" degradation in beryllides, silicides, aluminides and related compounds, *Journal of Nuclear Materials*, 12(2), 208(1964)
  5. J. X. Chen, C. H. Li, Z. Fu, X. Y. Tu, M. Sundberg, R. Pompe, Low-temperature oxidation behavior of a MoSi<sub>2</sub>-based material, *Materials Science and Engineering A*, 261(1-2), 239(1999)
  6. J. Kuchino, K. Kurokawa, T. Shibayama, H. Takahashi, Effect of microstructure on oxidation resistance of MoSi<sub>2</sub> fabricated by spark plasma sintering, *Vacuum*, 73(3-4), 623(2004)
  7. K. Kurokawa, H. Houzumi, I. Saeki, H. Takahashi, Low temperature oxidation of fully dense and porous MoSi<sub>2</sub>, *Materials Science and Engineering A*, 261, 292(1999)
  8. J. Arreguín-Zavala, S. Turenne, A. Martel, A. Benaissa, Microwave sintering of MoSi<sub>2</sub>-Mo<sub>5</sub>Si<sub>3</sub> to promote a final nanometer-scale microstructure and suppressing of pesting phenomenon, *Materials Characterization*, 68, 117(2012)
  9. K. Yanagihara, T. Maruyama, K. Nagata, Effect of third elements on the pesting suppression of Mo-Si-X intermetallics (X=Al, Ta, Ti, Zr and Y), *Intermetallics*, 4, S133(1996)
  10. T. Dasgupta, A. M. Umarji, Improved ductility and oxidation resistance in Nb and Al cosubstituted MoSi<sub>2</sub>, *Intermetallics*, 16(6), 739 (2008)
  11. E. Ström, Y. Cao, Y. M. Yao, Low temperature oxidation of Cr-alloyed MoSi<sub>2</sub>, *Transactions of Nonferrous Metals Society of China*, 17(6), 1282(2007)
  12. K. Natesan, S. C. Deevi, Oxidation behavior of molybdenum silicides and their composites, *Intermetallics*, 8, 1147(2000)
  13. ZHOU Hongming, LIU Gongqi, XIAO Lairong, YI Danqing, ZENG Lin, Low temperature oxidation behavior of MoSi<sub>2</sub> composites strengthened and toughened by Si<sub>3</sub>N<sub>4</sub> particles and SiC whiskers, *Journal of Inorganic Materials*, 24(5), 929(2009)
  14. K. Hansson, M. Halvarsson, J. E. Tang, Oxidation behaviour of a MoSi<sub>2</sub>-based composite in different atmospheres in the low temperature range (400-550°C), *Journal of the European Ceramic Society*, 24, 3559(2004)
  15. P. Z. Feng, X. H. Wang, Y. Q. He, Y. H. Qiang, Effect of high-temperature preoxidation treatment on the low-temperature oxidation behavior of a MoSi<sub>2</sub>-based composite at 500°C, *Journal of Alloys and Compounds*, 473(1-2), 185(2009)

16. YAN Jianhui, WANG Jinlin, TANG Siwen, In-situ synthesis and low temperature oxidation properties of TiC-MoSi<sub>2</sub> composites, Transaction of Materials and Heat Treatment, 32(1), 5(2011)
17. ZHANG Laiqi, SUN Zuqing, ZHANG Yue, YANG Wangyue, CHEN Guangnan, Microstructure and mechanical properties of in-situ SiC particulates reinforced MoSi<sub>2</sub> matrix composite, Acta Metallurgica Sinica, 37(3), 325(2001)
18. FU Xiaowei, YANG Wangyue, ZHANG Laiqi, SUN Zuqing, ZHU Jing, High temperature creep behavior of in-situ synthesized MoSi<sub>2</sub>-30%SiC composite, Acta Metallurgica Sinica, 38(7), 731(2002)
19. SUN Zuqing, ZHANG Laiqi, YANG Wangyue, ZHANG Yue, FU Xiaowei, A method of the preparation of in-situ silicon carbide particulates reinforced molybdenum disilicide matrix composites, China Patent, ZL01141978.4(2005)
20. ZHANG Laiqi, PAN Kunming, DUAN Lihui, LIN Junpin, Oxidation behavior of in-situ synthesized MoSi<sub>2</sub>-SiC composites at 500°C, Acta Metallurgica Sinica, 49(11), 1303(2013)
21. J. A. Lely, Silicon Carbide Semiconductor at High Temperature (Shanghai, Shanghai Science and Technology Press, 1962) p.138
22. T. C. Chou, T. G. Nieh, Mechanisms of MoSi<sub>2</sub> pest at 500°C, Scripta Metallurgica et Materialia, 27(1), 19(1992)
23. P. J. Meschter, Low-temperature oxidation of molybdenum disilicide, Metallurgical Transactions A, 23(6), 1763(1992)
24. T. A. Parthasarathy, M. G. Mendiratta, D. M. Dimiduk, Oxidation mechanisms in Mo-reinforced Mo<sub>5</sub>SiB<sub>2</sub>(T<sub>2</sub>)-Mo<sub>3</sub>Si alloys, Acta Materialia, 50(7), 1857(2002)

*Note: Figure translations are in progress. See original paper for figures.*

*Source: ChinaXiv – Machine translation. Verify with original.*